

**EFFECTS OF SPATIAL SCALE ON HOTSPOT ANALYSIS OF THE DENSITY
OF ANTARCTIC KRILL (*EUPHAUSIA SUPERBA*) IN
THE ANTARCTIC PENINSULA REGION**

H. Liu^{1,2}, G. Zhu^{1,2,3,4✉}

¹ College of Marine Sciences
Shanghai Ocean University
Shanghai 201306
China

² Center for Polar Research
Shanghai Ocean University
Shanghai 201306
China

³ Polar Marine Ecosystem Group
The Key Laboratory of Sustainable Exploitation
of Oceanic Fisheries Resources
Ministry of Education
Shanghai 201306
China

⁴ National Engineering Research Center
for Oceanic Fisheries
Shanghai 201306
China
E-mail: gpzhu@shou.edu.cn

Abstract

While the influence of spatial scale in ecology is well established, few studies have evaluated the impact of spatial scale on hotspot analysis of biological resources. Using data obtained from the KRILLBASE-ABUNDANCE database, this study aimed to investigate the effects of spatial scale on hotspot analysis of Antarctic krill (*Euphausia superba*) density distribution in the Antarctic Peninsula. Krill density data from 1929 to 2018 were interpolated at 10-year intervals into 10 spatial scales as follows: $10' \times 10'$, $20' \times 20'$, $30' \times 30'$, $40' \times 40'$, $50' \times 50'$, $1^\circ \times 1^\circ$, $2^\circ \times 2^\circ$, $3^\circ \times 3^\circ$, $4^\circ \times 4^\circ$ and $5^\circ \times 5^\circ$. Linear, logarithmic, exponential, power-law and parabolic functions were used to determine the relationship between spatial scale and krill density distribution in the Antarctic Peninsula region. Additionally, variations in centroid and area of hotspots at various spatial scales were analysed. The results revealed a strong scaling relationship between spatial scale, number of patches and indices of krill density. The hotspot area increased with an increase in the coarseness of the spatial scale and the calculated location of the centroid showed that the hotspot locations were markedly affected by the spatial scale of analysis, with coarser spatial scales resulting in larger spatial shifts in centroid location. Thus, based on the KRILLBASE-ABUNDANCE database, it is not recommended to use a spatial scale greater than $1^\circ \times 1^\circ$ to identify the local spatial pattern for hotspot analysis of krill density. The effects of spatial scale on other types of krill density data (e.g. catch data, acoustic data from research surveys or acoustic data from fishing vessels) remain to be investigated.

Résumé

Si l'influence de l'échelle spatiale en écologie est bien établie, peu d'études ont en revanche évalué l'impact de l'échelle spatiale sur l'analyse des zones de concentration de ressources biologiques. S'appuyant sur les données provenant de la base de données KRILLBASE-ABUNDANCE, cette étude a pour objectif d'étudier les effets de l'échelle spatiale sur l'analyse de la répartition de la densité de krill antarctique dans les zones de concentration (*Euphausia superba*) dans la péninsule antarctique. Les données de densité du krill de 1929 à 2018 sont interpolées par intervalles de 10 ans à 10 échelles spatiales comme suit : $10' \times 10'$, $20' \times 20'$, $30' \times 30'$, $40' \times 40'$, $50' \times 50'$, $1^\circ \times 1^\circ$, $2^\circ \times 2^\circ$, $3^\circ \times 3^\circ$, $4^\circ \times 4^\circ$ et $5^\circ \times 5^\circ$. Des fonctions linéaires, logarithmiques, exponentielles, de loi de puissance et paraboliques sont utilisées pour déterminer la relation entre l'échelle spatiale et la répartition de la densité de krill dans la région de la péninsule antarctique. En outre, les variations du centroïde et de l'aire des zones de concentration à différentes échelles spatiales sont analysées. Les résultats révèlent une forte relation d'échelle entre l'échelle spatiale, le nombre de regroupements et les indices de densité du krill. Plus l'échelle spatiale est approximative, plus la superficie de la zone de concentration augmente, et la position calculée du centroïde montre que l'échelle spatiale de l'analyse a une influence marquée sur la position des zones de concentration, le manque de précision des échelles spatiales ayant pour résultat de plus grands changements spatiaux de la position du centroïde. Ainsi, d'après la base de données KRILLBASE-ABUNDANCE, il n'est pas recommandé d'utiliser une échelle spatiale supérieure à $1^\circ \times 1^\circ$ pour identifier le schéma spatial local dans l'analyse des zones de concentration de la densité de krill. Les effets de l'échelle spatiale sur les autres types de données de densité du krill (p. ex. les données de capture, les données acoustiques issues des campagnes de recherche ou les données acoustiques des navires de pêche) doivent encore faire l'objet de recherches.

Абстракт

Влияние пространственного масштабирования в экологии хорошо известно, однако лишь немногие исследования посвящены оценке влияния пространственного масштаба на анализ очагов скопления биологических ресурсов. В данном исследовании, основанном на информации из базы данных KRILLBASE-ABUNDANCE, ставилась задача изучить влияние шкалы пространственного масштаба на анализ очагов скопления антарктического криля (*Euphausia superba*) вокруг Антарктического полуострова. Данные плотности криля с 1929 по 2018 гг. синхронно интерполировались с интервалом в 10 лет на шкалу 10 пространственных масштабов следующим образом: $10' \times 10'$, $20' \times 20'$, $30' \times 30'$, $40' \times 40'$, $50' \times 50'$, $1^\circ \times 1^\circ$, $2^\circ \times 2^\circ$, $3^\circ \times 3^\circ$, $4^\circ \times 4^\circ$ и $5^\circ \times 5^\circ$. Для определения зависимости между пространственным масштабом и распределением плотности криля в районе Антарктического полуострова использовались линейная, логарифмическая, экспоненциальная, степенная и параболическая функции. Кроме того, анализ подверглись изменения в расположении центроида и размерах очагов при раскладке на различные пространственные масштабы. Результаты выявили ярко выраженную пропорциональную зависимость между пространственным масштабом, количеством скоплений в очагах и индексами плотности криля. Площадь очагов скоплений увеличивалась с уменьшением точности пространственного масштаба, а рассчитанное местоположение центроида показало, что на расположение горячих точек заметно влияет пространственный масштаб анализа, где более грубые пространственные масштабы приводят к большим пространственным сдвигам в расположении центроида. Таким образом, основываясь на данные базы KRILLBASE-ABUNDANCE, не рекомендуется использовать пространственный масштаб превышающий $1^\circ \times 1^\circ$ для выявления особенностей пространственной структуры горячих точек при анализе плотности криля в очагах скоплений. Влияние пространственного масштаба на другие типы данных о плотности криля (напр., данные об уловах, акустические данные исследовательских съемок или акустические данные с промысловых судов) еще предстоит изучить.

Resumen

Si bien la influencia de la escala espacial en ecología está bien establecida, ha habido pocos estudios sobre el impacto de la escala espacial en el análisis de focos de abundancia de recursos biológicos. Utilizando datos obtenidos de la base de datos KRILLBASE-ABUNDANCE, el objetivo del presente estudio fue investigar los efectos de la escala espacial en el análisis de la distribución y la densidad de los focos de abundancia de kril antártico (*Euphausia superba*) en la península Antártica. Los datos de la densidad del kril desde 1929 hasta 2018 se agruparon por intervalos de 10 años en 10 escalas espaciales ($10' \times 10'$, $20' \times 20'$, $30' \times 30'$, $40' \times 40'$, $50' \times 50'$, $1^\circ \times 1^\circ$, $2^\circ \times 2^\circ$, $3^\circ \times 3^\circ$, $4^\circ \times 4^\circ$ y $5^\circ \times 5^\circ$). Se utilizaron funciones lineales, logarítmicas, exponenciales, potenciales y de parábolas para determinar el vínculo entre la escala espacial y la distribución de la densidad del kril en la región de la península Antártica. Además, se analizaron las variaciones en el centroide y en el área de los focos de abundancia en función de las escalas espaciales. Los resultados revelaron una fuerte relación escalar entre la escala espacial, el número de agrupaciones y los índices de la densidad del kril. El área de los focos de abundancia aumentaba en relación directa con la escala espacial, mientras que la ubicación calculada del centroide mostraba que las ubicaciones de los focos de abundancia se veían seriamente afectadas por la escala espacial del análisis; así, las escalas espaciales mayores resultaban en mayores desplazamientos espaciales de las ubicaciones del centroide. Por lo tanto, los datos de KRILLBASE-ABUNDANCE llevan a no recomendar la utilización de escalas espaciales superiores a $1^\circ \times 1^\circ$ para identificar las pautas espaciales locales en el análisis de la densidad del kril en focos de abundancia. Quedan pendientes de investigación los efectos de la escala espacial en otros tipos de datos de la densidad del kril (p. ej., datos de captura, datos acústicos de prospecciones de investigación o datos acústicos de barcos de pesca).

Introduction

Antarctic krill (*Euphausia superba*, hereafter referred to as krill) is an abundant crustacean widely distributed in the continental shelf waters of the Southern Ocean and primarily concentrated at depths shallower than 200 m, specifically in the waters surrounding the Antarctic Peninsula. Because of its extensive continental shelf and deep-sea canyon system, the waters off the Antarctic Peninsula are conducive to krill aggregation and residence. Krill mainly feeds on surface plankton, such as algae and tiny zooplankton (Schmidt et al., 2012). As a species with high biomass and a key species in the Southern Ocean ecosystem, krill has become an essential food source for high-trophic level predators in the Southern Ocean ecosystem (Nicol and Endo, 1999). The krill fishery is the most important fishery in the Southern Ocean (Santa Cruz et al., 2018; Weinstein et al., 2017; Kawaguchi and Nicol, 2007) and is managed by the Commission for the Conservation of Antarctic Marine Living Resources (CCAMLR).

Krill populations are distributed in a patchy manner throughout the entire Southern Ocean and form typical hotspots (areas with high-density krill swarms) in their preferred habits. However,

because of the varying temporal and spatial dynamics of krill distribution, research on the effects of the spatial scale of the analysis on estimates of krill density distribution has not made substantial progress. Nevertheless, many studies have shown that analysing habitats at various scales can provide insight into the distribution of biodiversity and community structure (Krawchuk and Taylor, 2003; Schmidt et al., 2008) and how spatial scales impact ecological processes (Thompson et al., 1996; Blanchard and Feder, 2014).

The relationships between a research objective and various factors derived at one spatial scale may be different or invalid at another spatial scale (Yang et al., 2021; Takashina and Baskett, 2016). If a model constructed at one spatial scale is applied to other scales without rigorous consideration, bias or errors can be introduced due to the differences in spatial scales. Thus, measuring change across spatial scales has always been a challenge in ecological studies (Turner et al., 1989; Wiens, 1989; Cushman et al., 2010). Many different spatial scales have been used to analyse the distribution of krill density. For example, Santa Cruz et al. (2018) processed the data from the krill fishery into a grid measuring 9×9 km, considering the

operational scale of the fishery. Perry et al. (2019) used a $2^\circ \times 1^\circ$ spatial scale to analyse the habitat distribution of krill at different life stages. Atkinson et al. (2008) used a $9^\circ \times 3^\circ$ spatial scale to examine the spatial distribution pattern of krill density and a $1^\circ \times 0.5^\circ$ spatial scale to determine the relationship between krill and environmental factors.

To date, few studies have been conducted on the effects of spatial scale on the description of the distribution of krill densities, making it difficult to compare the results of different studies. Moreover, if the data are used for analysis, important regions may be omitted or erroneous results may be produced (Zhang et al., 2014), thereby affecting decision-making for krill fishery management. Therefore, consideration of multiscale analysis is crucial for understanding spatial patterns in ecological processes. The analysis and discussion of the effects of spatial scale can have a strong impact on the accurate understanding of the relationship between spatial heterogeneity, spatial structure and spatial ecological processes and have substantial theoretical and practical value for evaluating ecological structure and biodiversity (Lammert and Allan, 1999; Peterson et al., 1998). Studies on spatial patterns of abundance are meaningful only when an appropriate scale is selected. Therefore, this study aimed to investigate the effect of spatial scale on the distribution of krill hotspots in the Antarctic Peninsula and evaluated scale effects from two aspects, –krill density statistics and spatial indices (including hotspot area and hotspot centroid)– to provide fundamental data for analysis of krill distribution and to facilitate the management of krill.

Materials and Methods

Data collection

All data were obtained from the KRILLBASE-ABUNDANCE database, which contains integrated data of multinational Antarctic circumpolar surveys (Atkinson et al., 2017). The database primarily contains krill survey data from 1926 to 2018, including survey time, location and krill standardised density estimates. Although different sampling methods were used in the surveys owing to differences in the scales and types of data sources, the density of krill was standardised (ind m^{-2}) (Atkinson et al., 2008). The survey stations that collected krill density data

near the Antarctic Peninsula are shown in Figure 1. In this study, the krill density near the Antarctic Peninsula was divided into various 10-year interval periods, and the years included in each period are listed in Table 1. Some years were missed because no data were available.

Hotspot analysis

Spatial scales include the resolution and extent of species distribution (Wu and Li, 2006), and the spatial scale investigated in this study was resolution. Moreover, the resolution was set to a fine scale (less than $1^\circ \times 1^\circ$) with a small step size ($10'$), whereas on a large scale (greater than $1^\circ \times 1^\circ$), the step size was 1° . The original data were interpolated to spatial scales of $10' \times 10'$, $20' \times 20'$, $30' \times 30'$, $40' \times 40'$, $50' \times 50'$, $1^\circ \times 1^\circ$, $2^\circ \times 2^\circ$, $3^\circ \times 3^\circ$, $4^\circ \times 4^\circ$ and $5^\circ \times 5^\circ$. From the landscape ecology perspective (Forman and Godron, 1981), the concept of a ‘patch’ was described as a grid cell. The krill density in each patch was determined as the sum of krill density observations divided by the number of krill density survey stations in the patch.

A single observation with a high (or low) value is not necessarily a statistically significant hotspot (or coldspot). The most widely used local spatial autocorrelation statistical analysis is hotspot analysis based on Getis-Ord G_i^* , which identifies hotspots (or coldspots) as spatial clusters with statistically significant high (or low) z-score values (Ord and Getis, 1995). Therefore, in a hotspot analysis, a hotspot is an area where high-value observations of krill density are surrounded by other high-density observations, whereas a coldspot appears as a low-value observation surrounded by other low-value observations. In this study, hotspot analysis was performed using the ArcGIS 10.5 software and spatial relationships were conceptualised using a fixed-distance band. A 95% confidence interval ($p < 0.05$) was used to determine hotspots and coldspots, with the patch considered a hotspot or coldspot if the z-score was >1.96 or <-1.96 respectively.

The z-score is given as (Ord and Getis, 1995)

$$z_i = \frac{\sum_{j=1}^n w_{i,j} x_j - \bar{X} \sum_{j=1}^n w_{i,j}}{S \sqrt{\frac{n \sum_{j=1}^n w_{i,j}^2 - (\sum_{j=1}^n w_{i,j})^2}{n-1}}}$$

$$\bar{X} = \frac{\sum_{j=1}^n x_j}{n}$$

$$S = \sqrt{\frac{\sum_{j=1}^n x_j^2}{n} - (\bar{X})^2} \quad (1)$$

where n is the total number of stations, x_j is the krill density for station j and w_{ij} is the spatial weight between station i and j calculated by a fixed-distance band.

Indices of measuring the scaling relationship

To determine the effect of spatial scale on krill density distribution for all stations and hotspots, five indices of krill density for each spatial scale were calculated: average, standard deviation (SD), skewness, kurtosis of krill density for all patches and number of patches. The number of patches is a common index in landscape ecology study (Bowers and Matter, 1997; Flick et al., 2012; Crouzeilles et al., 2014). Calculating the average is a common method for gridding irregular point data in many studies (Santa Cruz et al., 2018; Perry et al., 2019; Atkinson et al., 2008; Harvey et al., 2017; Kuletz et al., 2015). The change of data probability distribution was not considered when data is gridded in some studies, but the data distribution varied with the change in spatial scale. While kurtosis and skewness were indices of data distribution, SD reflected the degree of dispersion of data. Spatial indices such as spatial area and centroid of hotspots for each spatial scale were also determined to analyse changes in the spatial distribution of krill hotspots caused by changes in the spatial scale. For each period and each spatial scale, after the hotspots were identified via hotspot analysis, multiple hotspots were merged into a polygon (a large hotspot) in ArcGIS and the centroid and area of the resulting polygon were determined.

To evaluate the scale effect of these indices, linear, logarithmic, exponential, power-law and parabolic regression models were used (Table 2). Among the candidate models, the most suitable model was selected using the corrected Akaike information criterion (AICc), where the model with the smallest AICc value represents the best model (Burnham et al., 2011). Model fitting was completed using a fitting function in MATLAB R2020a (Duc-Toan et al.,

2012; Dubey et al., 2016; Kurniawan et al., 2020). For linear, logarithmic and exponential functions, $a > 0$ and $a < 0$ indicate an increasing and decreasing trend of the index respectively, with an increase in the spatial scale. Owing to changes in the spatial scale, the fractal dimension (d) was calculated to quantify the degree of change in the index for the power-law function. A $|d|$ close to 1 indicates that the index is not sensitive to changes in the spatial scale, whereas $|d| \geq 1.3$ indicates that the index is sensitive to changes in the spatial scale (Feng et al., 2019). Fractal dimension was calculated as follows (Feng and Liu, 2015).

$$d = \begin{cases} \frac{1-a}{-1-a}, & a < 0 \\ -1-a, & a \geq 0 \end{cases} \quad (2)$$

Results

Scale effect of krill density distribution for all stations

The number of patches, SD, skewness and kurtosis showed a decreasing trend with an increase in the spatial scale. The average showed an overall increasing trend (Figure 2). With an increase in the spatial scale, the skewness decreased, and the krill density gradually approached a normal distribution. Additionally, kurtosis decreased with an increase in the spatial scale, where it changed from sharp kurtosis to low kurtosis, indicating a change in the krill density (Figure 3).

Table 3 presents the indices and periods with high coefficients of determination ($R^2 \geq 0.7$). Except for a few periods, there was a strong proportional relationship between the five indices and the spatial scale. The relationship between the number of patches and the spatial scale was generally exponential in nature. The SD and the spatial scale followed a power-law relationship. The relationship between skewness and spatial scale was exponential or parabolic in nature. The relationship between kurtosis and spatial scale was primarily exponential in nature. In all periods, a linear relationship had never been observed. The fitted equations indicated an unusually strong correlation between the number of patches and the spatial scale in each period, and the coefficients of determination were all above 0.98. Except for the average,

the $|d|$ of the other indices were all greater than 1.3 (Table 3), indicating that these non-spatial indices were sensitive to changes in spatial scales.

Scale effects of nonspatial indices on hotspots

At the spatial scale of $5^\circ \times 5^\circ$, there was no hotspot during any period, and at the spatial scale of $10' \times 10' \sim 1^\circ \times 1^\circ$, there were hotspots in all periods (Table 4). At the scale of $3^\circ \times 3^\circ$ from 1929 to 1938, the scale of $50' \times 50'$ from 1969 to 1978, the scale of $3^\circ \times 3^\circ$ from 1979 to 1988, the scale of $4^\circ \times 4^\circ$ from 1989 to 1998, the $2^\circ \times 2^\circ$ and $4^\circ \times 4^\circ$ scales from 1999 to 2008 and the $3^\circ \times 3^\circ$ scale from 2009 to 2018 all had only one hotspot (Table 4). Therefore, except for the number of patches, other indices were not found to be fitted to the spatial scale at these scales in these periods. Additionally, there was no hotspot at the scale of $2^\circ \times 2^\circ$, $3^\circ \times 3^\circ$ and $4^\circ \times 4^\circ$ from 1969 to 1978, the scale of $4^\circ \times 4^\circ$ from 1979 to 1988, the scale of $2^\circ \times 2^\circ$ from 1989 to 1998 and the scale of $3^\circ \times 3^\circ$ from 1999 to 2008 (Table 4). Nevertheless, coldspots existed only at the scale of $10' \times 10'$ and $40' \times 40'$ from 1969 to 1978, the scale of $3^\circ \times 3^\circ$ from 1979 to 1988 and the scale of $60' \times 60'$ from 2006 to 2018 (Table 4). For considering the number of samples needed for statistical analysis, coldspots were not analysed in this study.

With an increase in the spatial scale, the numbers of patches, SD, skewness and kurtosis of hotspots indicated a general downward trend (Figure 4). This was similar to the situation for krill densities of all stations. The average showed an increasing trend first, which then decreased with an increase in the spatial scale.

For hotspots, there were strong correlations between the remaining indices and the spatial scale except for the average. The relationship of spatial scale with the numbers of patches, SD, skewness and kurtosis of krill density was primarily parabolic or power-law in nature (Table 5). The $|d|$ of SD, kurtosis and numbers of patches were all greater than 1.3 (Table 5), indicating that the three indices of krill hotspots are also sensitive to changes in spatial scales.

Scale effects of spatial indices of hotspots

The centroid represents the location of the hotspots. The locations of the hotspots in the same period differed at different spatial scales and considerable differences were found during some periods (Figure 6). From 1929 to 1938, the hotspots appeared in southern waters around Elephant Island and the centroid of the hotspots was shifted by $1.5^\circ \times 2.5^\circ$ as a whole (Figure 6a). The offset of the centroid of the hotspots was small within a scale finer than $1^\circ \times 1^\circ$. When the spatial scale was greater than $1^\circ \times 1^\circ$, the centroid of the hotspots was shifted markedly, and the offset range of the centroid of the latter was 36 times that of the former. The hotspots also appeared northeast of the Bransfield Strait from 1969 to 1978. The centroid of the hotspots moved along the southwest–northeast direction generally with an increase in the spatial scale, with an overall offset of $4.3^\circ \times 2.3^\circ$ (Figure 6b). From 1979 to 1988, the hotspots appeared southwest of the Bransfield Strait (Figure 6c). The centroid of the hotspots was primarily shifted in the zonal direction, and the southerly direction was less, with a general offset of $9.5^\circ \times 0.7^\circ$. From 1989 to 1998, the hotspots appeared northeast of the Bransfield Strait (Figure 6d). The centroid of the hotspots was shifted by $3.5^\circ \times 1.4^\circ$ as a whole, with obvious offset at each spatial scale. From 1999 to 2008, the hotspots appeared in the middle of the Bransfield Strait and the centroid of the hotspots was shifted by $6.1^\circ \times 1.4^\circ$ as a whole (Figure 6e). At a scale finer than $1^\circ \times 1^\circ$, the offset of the centroid of the hotspots was primarily concentrated in the zonal direction. The hotspots appeared in the middle of the Bransfield Strait from 2009 to 2018 and the centroid of the hotspots was shifted by $4^\circ \times 1.2^\circ$ (Figure 6f). At a scale larger than $1^\circ \times 1^\circ$, the offset range of the centroid was 20 times larger than that at scales smaller than $1^\circ \times 1^\circ$.

This study showed that around the Antarctic Peninsula at a scale of $10' \times 10' - 5^\circ \times 5^\circ$, there were no coldspots in the waters. Hotspots appeared in the southwest, northeast and middle of the Bransfield Strait. The hotspots that appeared in the northwest of the Bransfield Strait from 1929 to 1938 and from 1969 to 1978 were the same hotspot and the hotspots that appeared in the middle of the Bransfield Strait from 1999 to 2008 and from 2009 to 2018 were deemed to be the same hotspot. The spatial clustering time of hotspots in the northeastern and

central Bransfield Strait (1929–1938, 1968–1978, 1999–2008 and 2009–2018) was more persistent than that in the southwestern Bransfield Strait.

As the spatial scale increased, although the number of hotspots decreased, the area of a single hotspot increased. The hotspot area also showed an increasing trend in general (Figure 7). From 1969 to 1978, there was no strong correlation between the hotspot area and the spatial scale. There was an exponential relationship between the hotspot area and the spatial scale from 1929 to 1938, 1999 to 2008 and 2009 to 2018. From 1979 to 1988 and from 1989 to 1998, there was a parabolic relationship between the hotspot area and the spatial scale (Table 6).

Discussion

Scale effect

The original scientific survey and fishery data were in point format, specifically fishery data, and the data were collected irregularly. Previous studies converted the data into a standard grid form before conducting hotspot analysis. For example, Harvey et al. (2017) processed the marine survey data into a regular hexagon with an area of 13.86 km^2 to match the environmental data. Kuletz et al. (2015) processed the data into a $40 \times 40 \text{ km}$ grid to ensure a sufficient sample number in each grid. Through multiscale analyses of the krill density data from 1929 to 2018, it can be found that both the spatial patterns of krill density distribution in the entire survey area and the spatial patterns of krill hotspots were considerably affected by the spatial scale. Our results showed there are various proportional relationships between spatial scales and in indices, including logarithmic, exponential, power-law and parabolic scaling relationships. A linear relationship between each index and spatial scale was not found in any period. With an increase in the spatial scale, the number of patches in the entire survey area and the number of patches of hotspots showed a decreasing trend.

Additionally, linear function, logarithmic, exponential, power-law and parabolic functions all had good fitting effects on the relationship between the number of patches and the spatial scale. The lowest coefficient of determination was 0.7. In existing ecological research, species number and

sampling areas are the oldest and most abundant among the recorded indices, and these indices are strongly scale-dependent (Palmer and White, 1994; Crawley and Harral, 2001). Compared with the fluctuation of nonspatial indices of krill density in the entire survey area, the fluctuation of the nonspatial indices of krill hotspot densities was more prominent. Moreover, there was no simple upward or downward relationship with the spatial scale, indicating that the spatial scale had a more complex impact on krill hotspots. The results also showed that the centroids of hotspots varied with the spatial scale, and there were marked differences in the location of hotspots at different spatial scales. Except for the 1969–1978 period, there was a high positive correlation between the hotspot area and the spatial scale. However, the offset trajectory of the centroids did not show any evident regularity in terms of offset direction or offset range.

Continuity and time persistence of hotspots

Spatial statistical methods (Getis-Ord G_i^*) were used to identify hotspots and coldspots of krill densities. At the fine scale, irrespective of the year, all the hotspots appeared in the interior of Bransfield Strait. The seas around the Antarctic Peninsula were characterised by complex currents, with upwelling and frontal zones, and the extended continental shelf and complex ocean currents provided good food sources for krill in the Bransfield Strait. These oceanographic features and topographical structures provided favourable conditions for the accumulation of krill, which were conducive to krill establishing habitats and forming hotspots in the Bransfield Strait (Sokolov and Rintoul, 2007). From the perspective of time change, the hotspots observed northwest of the Bransfield Strait existed at the scale of $10' \times 10' - 1^\circ \times 1^\circ$. The hotspots in the middle of the Bransfield Strait existed at the scale of $10' \times 10' - 4^\circ \times 4^\circ$ (except for $2^\circ \times 2^\circ$), but the spatial position changed owing to the differences in spatial scales.

Conversely, the temporal persistence of hotspots remains consistent at various spatial scales. Therefore, it is possible to speculate that the temporal persistence of hotspots is not affected by the spatial scale or is less affected. No hotspot was found at large spatial scales during the same period. For example, during the 1989–1998 period, no hotspot was found at a scale of $2^\circ \times 2^\circ$, and during the 1999–2008 period, no hotspot was found at a scale

of $3^\circ \times 3^\circ$. However, these hotspots existed at other smaller and larger spatial scales. In 1999–2008 and 2009–2018, the centroid of hotspots appeared on the Antarctic Peninsula at a scale of $2^\circ \times 2^\circ$. Because the latitude of the entire study area differed by only five degrees (60°S – 65°S), when the spatial scale was large ($2^\circ \times 2^\circ$), the grid would inevitably cover portions of land. Therefore, a large spatial scale was not conducive to determining the variation in the spatial distribution of krill. Additionally, it can be seen from the decrease in SD with an increase in spatial scale that the spatial pattern of krill density tended to be homogenised with an increase in the spatial scale. Furthermore, concealing the original spatial distribution data of krill densities may result in erroneous results if the study is conducted on a very large scale. Judging from the offset extent of the centroids, the centroids of hotspots at scales larger than $1^\circ \times 1^\circ$ were markedly different from those at smaller scales. Therefore, it is not appropriate to use a spatial scale larger than $1^\circ \times 1^\circ$ to determine the spatial pattern of krill densities in the waters around the Antarctic Peninsula.

The data collected over a short time period, such as months, is not suitable for studying scale effects owing to the greater possibility of variation. Using data from longer periods was helpful for understanding the scaling of krill distribution. Additionally, the spatial scale in degrees ($^\circ$) and minutes ($'$) is different from the spatial scale in kilometres, and the longitude length of grid cell varies with latitude, but in theory it does not affect the results of the study. This is because if the longitude and latitude were replaced by the spatial scale in kilometres, the trends in the basic statistics of krill density and krill hotspots with changes in spatial scale should theoretically be the same. For example, the kurtosis, skewness of krill densities and number of patches should be decreased with an increasing spatial scale, and the centroid of hotspots should show a smaller shift in the fine scale and a larger shift in the coarse scale.

However, this study was based on data derived from the KRILLBASE-ABUNDANCE database, and only the scale effect of krill density in the Antarctic Peninsula was analysed. Therefore, further studies are required if the results are extended to other regions or other types of krill data (e.g. catch data, acoustic data from research surveys and acoustic data from fishing vessels) are used. In addition, the ‘fit’ function was used in MATLAB

to analyse the variation of each index with spatial scale and to obtain the specific parameters of fitted models – that is, (a) and (b) in Table 2 – but the specific parameters of models may be slightly different depending on the fitting method, such as the generalised additive model.

Conclusion

The average, SD, skewness, kurtosis of krill density and numbers of patches in the waters around the Antarctic Peninsula were different at scales of $10' \times 10'$, $20' \times 20'$, $30' \times 30'$, $40' \times 40'$, $50' \times 50'$, $1^\circ \times 1^\circ$, $2^\circ \times 2^\circ$, $3^\circ \times 3^\circ$, $4^\circ \times 4^\circ$ and $5^\circ \times 5^\circ$. These nonspatial indices and hotspot area were strongly proportional to the spatial scale. Therefore, the spatial scale substantially impacted the hotspot’s location. During most periods, the offset of the hotspot centroid was not evident at a spatial scale less than $1^\circ \times 1^\circ$. However, when the spatial scale was greater than $1^\circ \times 1^\circ$, the centroid of the hotspot shifted markedly. Therefore, it is not recommended to use a spatial scale greater than $1^\circ \times 1^\circ$ to identify the fine-scale spatial pattern of krill density in the Antarctic Peninsula region.

Acknowledgments

We thank the British Antarctic Survey for providing the KRILLBASE-ABUNDANCE data and the technical staff involved in the field survey for their extensive support for this study. We also thank the College of Marine Sciences at the Shanghai Ocean University for providing the laboratory facilities that allowed us to conduct this study. Funding was provided by the International Science and Technology Cooperation Key Special Project of the National Key Research and Development Program (grant no. 2023YFE0104500 to GPZ), the Promote scientific research cooperation and high-level talent training projects with Canada, Australia, New Zealand and Latin America, the Chinese Scholarship Council (grant no. 2021-109 to GPZ), and the National Science Foundation of China (grant no. 41776185 to GPZ).

References

- Atkinson, A., V. Siegel, E.A. Pakhomov, P. Rothery, V. Loeb, R.M. Ross, L.B. Quetin, K., Schmidt, P. Fretwell, E.J. Murphy, G.A. Tarling and

- A.H. Fleming. 2008. Oceanic circumpolar habitats of Antarctic krill. *Mar. Ecol. Prog. Ser.*, 362: 1–23, doi: 10.3354/meps07498.
- Atkinson, A., S.L. Hill, E.A. Pakhomov, V. Siegel, R. Anadon, S. Chiba, K.L. Daly, R. Downie, S. Fielding, P. Fretwell, L. Gerrish, G.W. Hosie, M.J. Jessopp, S. Kawaguchi, B.A. Kraft, V. Loeb, J. Nishikawa, H.J. Peat, C.S. Reiss, R.M. Ross, L.B. Quetin, K. Schmidt, D.K. Steinberg, R.C. Subramaniam, G.A. Tarling and P. Ward. 2017. KRILLBASE: A database of Antarctic krill and sulp densities in the Southern Ocean, 1926 to 2016. *Earth Syst. Sci. Data*, 9: 193–210, doi: <https://doi.org/10.5194/essd-9-193-2017>.
- Blanchard, A.L. and H.M. Feder. 2014. Interactions of habitat complexity and environmental characteristics with macrobenthic community structure at multiple spatial scales in the northeastern Chukchi Sea. *Deep-Sea Res. II*, 102: 132–143, doi: 10.1016/j.dsr2.2013.09.022.
- Bowers, M.A. and S.F. Matter. 1997. Landscape ecology of mammals: Relationships between density and patch size. *J. Mammal.*, 78(4): 999–1013, doi: 10.2307/1383044.
- Burnham, K.P., D.R. Anderson and K.P. Huyvaert. 2011. AIC model selection and multimodel inference in behavioral ecology: Some background, observations, and comparisons. *Behav. Ecol. Sociobiol.*, 65: 23–35, doi: 10.1007/s00265-010-1084-z.
- Crawley, M.J. and J.E. Harral. 2001. Scale dependence in plant biodiversity. *Science*, 291 (5505): 864–868.
- Crouzeilles, R., J.A. Prevedello, M.D.L. Figueiredo, M.L. Lorini and C.E.V. Grelle. 2014. The effects of the number, size and isolation of patches along a gradient of native vegetation cover: how can we increment habitat availability? *Landsc. Ecol.*, 29 (3): 479–489, doi: 10.1007/s10980-013-9978-6.
- Cushman, S.A., J. Littell, and K. McGarigal. 2010. The problem of ecological scaling in spatially complex, nonequilibrium ecological systems. In: Cushman, S.A., Huettmann, F. (Eds). *Spatial Complexity, Informatics, and Wildlife Conservation*. Springer, Tokyo: 43–63.
- Dubey S., D. Gusain and Y.C. Sharma. 2016. Kinetic and isotherm parameter determination for the removal of chromium from aqueous solutions by nanoalumina, a nanoadsorbent. *J. Mol. Liq.*, 219: 1–8.
- Duc-Toan N., B. Tien-Long, J. Dong-Won, Y. Seung-Han and K. Young-Suk. 2012. A modified Johnson-Cook model to predict stress-strain curves of Boron steel sheets at elevated and cooling temperatures. *High Temp. Mater. Process.*, 31 (1): 37–45, doi: <https://doi.org/10.1515/htmp.2011.127>.
- Feng, Y.J. and Y. Liu. 2015. Fractal dimension as an indicator for quantifying the effects of changing spatial scales on landscape metrics. *Ecol. Indic.*, 53: 18–27.
- Feng, Y.J., L.J. Chen and X.J. Chen, X.J. 2019. The impact of spatial scale on local Moran's I clustering of annual fishing effort for *Dosidicus gigas* offshore Peru. *J. Oceanol. Limnol.*, 37 (1): 330–343.
- Flick, T., S. Feagan and L. Fahrig. 2012. Effects of landscape structure on butterfly species richness and abundance in agricultural landscapes in eastern Ontario, Canada. *Agric. Ecosyst. Environ.*, 156: 123–133, doi: 10.1016/j.agee.2012.05.006.
- Forman, R.T.T. and M. Godron. 1981. Patches and structural components for a landscape ecology. *BioScience*, 31 (10): 733–740, doi: <https://doi.org/10.2307/1308780>.
- Harvey, G.K.A., T.A. Nelson, C.H. Fox and P.C. Paquet. 2017. Quantifying marine mammal hotspots in British Columbia, Canada. *Ecosphere*, 8 (7): e01884, doi: 10.1002/ecs2.1884.
- Kawaguchi, S. and S. Nicol. 2007. Learning about Antarctic krill from the fishery. *Ant. Sci.*, 19 (2): 219–230, doi: 10.1017/S0954102007000296.
- Krawchuk, M.A. and P.D. Taylor. 2003. Changing importance of habitat structure across multiple spatial scales for three species of insects. *Oikos*, 103 (1): 153–161, doi: <https://doi.org/10.1034/j.1600-0706.2003.12487.x>.

- Kuletz, K.J., M.C. Ferguson, B. Hurley, A.E. Gall, E.A. Labunski and T.C. Morgan. 2015. Seasonal spatial patterns in seabird and marine mammal distribution in the eastern Chukchi and western Beaufort seas: Identifying biologically important pelagic areas. *Prog. Oceanogr.*, 136: 175–200, doi: 10.1016/j.pocean.2015.05.012.
- Kurniawan A., K. Abe, M. Sanada, T. Nomura and T. Akiyama. 2020. Kinetic study of simultaneous ethanol decomposition and reduction of low-grade iron ore at transient temperature. *IOP Conf. Ser. Mater. Sci. Eng.*, 778 (1): 012056, doi: 10.1088/1757-899X/778/1/012056.
- Lammert, M. and J.D. Allan. 1999. Assessing biotic integrity of streams: Effects of scale in measuring the influence of land use/cover and habitat structure on fish and macroinvertebrates. *Environ. Manage.*, 23 (2): 257–270, doi: <https://doi.org/10.1007/s002679900184>.
- Nicol, S. and Y. Endo. 1999. Krill fisheries: Development, management and ecosystem implications. *Aquat. Living Resour.*, 12 (2): 105–120.
- Ord, J.K. and A. Getis. 1995. Local spatial autocorrelation statistics: Distributional issues and an application. *Geogr. Anal.*, 27: 286–306, doi: 10.1111/j.1538-4632.1995.tb00912.x.
- Palmer, M.W. and P.S. White. 1994. Scale dependence and the species-area relationship. *Am. Nat.*, 144 (5): 717–740, doi: 10.1086/285704.
- Perry, F.A., A. Atkinson, S.F. Sailley, G.A. Tarling, S.L. Hill, C.H. Lucas and D.J. Mayor. 2019. Habitat partitioning in Antarctic krill: Spawning hotspots and nursery areas. *PLOS One*, 14 (7): e0219325, doi: <https://doi.org/10.1371/journal.pone.0219325>.
- Peterson, G., C.R. Allen and C.S. Holling. 1998. Ecological resilience, biodiversity, and scale. *Ecosystems*, 1: 6–18, doi: 10.1007/s100219900002.
- Santa Cruz, F., B. Ernst, J.A. Arata, and C. Parada. 2018. Spatial and temporal dynamics of the Antarctic krill fishery in fishing hotspots in the Bransfield Strait and South Shetland Islands. *Fish. Res.*, 208: 157–166, doi: 10.1016/j.fishres.2018.07.020.
- Schmidt, K., A. Atkinson, H.J. Venables and D.W. Pond. 2012. Early spawning of Antarctic krill in the Scotia Sea is fuelled by “superfluous” feeding on non-ice associated phytoplankton blooms. *Deep-Sea Res. II*, 59: 159–172, doi: 10.1016/j.dsr2.2011.05.002.
- Sokolov, S. and S.R. Rintoul. 2007. On the relationship between fronts of the Antarctic Circumpolar Current and surface chlorophyll concentrations in the Southern Ocean. *J. Geophys. Res. Oceans*, 112 (C7): C07030, doi:10.1029/2006JC004072.
- Takashina, N. and M.L. Baskett. 2016. Exploring the effect of the spatial scale of fishery management. *J. Theor. Biol.*, 390: 14–22, doi: 10.1016/j.jtbi.2015.11.005.
- Thies, C., I. Steffan-Dewenter and T. Tscharntke. 2003. Effects of landscape context on herbivory and parasitism at different spatial scales. *Oikos*, 101 (1): 18–25, doi: 10.1034/j.1600-0706.2003.12567.x.
- Thompson, R.C., B.J. Wilson, B.M.L. Tobin, A.S. Hill and S.J. Hawkins. 1996. Biologically generated habitat provision and diversity of rocky shore organisms at a hierarchy of spatial scales. *J. Exp. Mar. Biol. Ecol.*, 202 (1): 73–84.
- Turner, M.G., R.V. O'Neill, R.H. Gardner and B.T. Milne. 1989. Effects of changing spatial scale on the analysis of landscape pattern. *Landsc. Ecol.*, 3: 153–162, doi: <https://doi.org/10.1007/BF00131534>.
- Weinstein, B.G., M. Double, N. Gales, D.W. Johnston and A.S. Friedlaender. 2017. Identifying overlap between humpback whale foraging grounds and the Antarctic krill fishery. *Biol. Conserv.*, 210: 184–191, doi: 10.1016/j.biocon.2017.04.014.
- Wiens, J.A. 1989. Spatial scaling in ecology. *Funct. Ecol.*, 3 (4): 385–397, doi: <http://dx.doi.org/10.2307/2389612>.
- Wu, J. and H. Li. 2006. Concepts of scale and scaling. In: Wu, J., K.B. Jones, H. Li and O.L. Loucks. (Eds). *Scaling and uncertainty analysis in ecology*. Springer, Dordrechtand–15, doi: 10.1007/1-4020-4663-4_1.

Yang, M.H., X.D. Gao, X.N. Zhao and P.T. Wu,. 2021. Scale effect and spatially explicit drivers of interactions between ecosystem services—A case study from the Loess Plateau. *Sci. Total. Environ.*, 785: 147389, doi: 10.1016/j.scitotenv.2021.147389.

Zhang, J.X., P. Atkinson and M.F. Goodchild. 2014. Scale in spatial information and analysis. *CRC Press*, Boca Raton: 1–16.

Table 1: Survey periods and sample size of krill density data collection in the waters around the Antarctic Peninsula (data source: KRILLBASE-ABUNDANCE).

Period	Years with available data for estimation	Number of stations
1929–1938	1929/1930/1931/1932/1933/1934/1938	102
1969–1978	1976/1978	225
1979–1988	1981/1982/1983/1984/1985/1987/1988	876
1989–1998	1989/1990/1991/1992/1993/1994/1995/1996/1997/1998	1769
1999–2008	1999/2000/2001/2002/2003/2004/2005/2006/2007/2008	1794
2009–2018	2009/2010/2011/2012/2013/2014/2015/2016	300

Table 2: The regression models used to evaluate the scale effect of indices. Y denotes the index; x denotes the spatial scale (unit of x is ').

Scaling relation	Equation
Linear	$y = a*x + b$
Logarithmic	$y = a*\ln x + b$
Exponential	$y = b^*e^{ax}$
Power-law	$y = b^*x^a$
Parabolic	$y = a_2x^2 + a_1x + a_0$

Table 3: Fitted equations of indices and spatial scales (unit of x is ').

Index	Period	Fitted equation	Scaling relation	Coefficient of determination (R^2)	Degrees of freedom	d
Number of patches	1929–1938	$y = -24.636\ln(x) + 141.688$	logarithmic	0.991	8	-
	1969–1978	$y = 175.086e^{-0.021x}$	exponential	0.992	8	-
	1979–1988	$y = 627.471e^{-0.042x}$	exponential	0.992	8	-
	1989–1998	$y = 4739.549x^{-1.044}$	Power-law	0.992	8	2.044
	1999–2008	$y = 498.722e^{-0.041x}$	exponential	0.992	8	-
	2009–2018	$y = 261.421e^{-0.032x}$	exponential	0.989	8	-
Average	1969–1978	$y = 61.109e^{0.003x}$	exponential	0.884	8	-
	1999–2008	$y = -3.664 \times 10^{-5}x^2 - 0.038x + 28.243$	parabolic	0.788	7	-
SD	1929–1938	$y = 0.007x^2 - 2.674x + 310.156$	parabolic	0.762	7	-
	1979–1988	$y = -87.709\ln(x) + 499.242$	logarithmic	0.916	8	-
Skewness	1989–1998	$y = 2710.254x^{-1.154}$	power-law	0.966	8	2.154
	1999–2008	$y = 642.236x^{-0.682}$	power-law	0.950	8	1.682
	1929–1938	$y = 7.311e^{-0.007x}$	exponential	0.929	8	-
	1969–1978	$y = 3.688 \times 10^{-5}x^2 - 0.03x + 6.891$	parabolic	0.930	7	-
	1979–1988	$y = 1.081 \times 10^{-4}x^2 - 0.057x + 7.199$	parabolic	0.942	7	-
	1989–1998	$y = 114.817x^{-0.957}$	power-law	0.943	8	1.957
Kurtosis	1999–2008	$y = 15.902e^{-0.034x}$	exponential	0.880	8	-
	2009–2018	$y = -3.767\ln(x) + 21.489$	logarithmic	0.974	8	-
	1929–1938	$y = 58.859e^{-0.013x}$	exponential	0.897	8	-
	1969–1978	$y = 62.350e^{-0.011x}$	exponential	0.922	8	-
	1979–1988	$y = 0.001x^2 - 0.502x + 53.131$	parabolic	0.804	7	-
	1989–1998	$y = 13181.597x^{-1.829}$	power-law	0.988	8	2.829
2009–2018	1999–2008	$y = 242.549e^{-0.053x}$	exponential	0.829	8	-
	2009–2018	$y = 216.771e^{-0.03x}$	exponential	0.985	8	-

Note: The symbol ‘-’ indicates that there is no fractal dimension (d).

Table 4: The number of patches across spatial scales during different periods.

Type of patch	Period	Spatial scale									
		10'	20'	30'	40'	50'	1°	2°	3°	4°	5°
Hotspot	1929–1938	12	9	6	6	6	4	3	1	2	0
	1969–1978	2	7	7	5	1	3	0	0	0	0
	1979–1988	30	28	13	7	8	7	3	1	0	0
	1989–1998	34	14	8	6	4	3	0	2	1	0
	1999–2008	27	19	2	14	8	7	1	0	1	0
	2009–2018	11	10	5	5	6	5	3	1	2	0
Coldspot	1969–1978	1	0	0	1	0	0	0	0	0	0
	1979–1988	0	0	0	0	0	0	0	1	0	0
	2009–2018	0	0	0	0	0	1	0	0	0	0

Table 5: Fitted equations of indices of hotspots and spatial scales (unit of x is ').

Index	Period	Fitted equation	Scaling relation	Coefficient of determination (R^2)	Degrees of freedom	d
Number of patches	1929–1938	$y = 46.848x^{-0.577}$	power-law	0.955	7	1.577
	1979–1988	$y = 45.72e^{-0.036x}$	exponential	0.921	6	-
	1989–1998	$y = 658.207x^{-1.287}$	power-law	0.998	6	2.287
	1999–2008	$y = 196.259x^{-0.853}$	power-law	0.791	6	1.853
	2009–2018	$y = 41.107x^{-0.545}$	power-law	0.885	7	1.545
SD	1929–1938	$y = 0.020x^2 - 8.136x + 843.644$	parabolic	0.708	5	-
	1979–1988	$y = 3.445 \cdot 10^{-4}x^2 - 4.377x + 573.651$	parabolic	0.700	4	-
	1989–1998	$y = 11658.683x^{-1.322}$	power-law	0.972	5	2.322
	1999–2008	$y = -0.016x^2 - 4.593x + 348.03$	parabolic	0.808	3	-
	2009–2018	$y = 1.119 \cdot 10^{-4}x^2 - 0.039x + 2.989$	parabolic	0.968	5	-
Skewness	1929–1938	$y = -0.975\ln(x) + 5.33$	logarithmic	0.718	5	-
	1979–1988	$y = 10.984e^{-0.071x}$	exponential	0.981	5	-
	1989–1998	$y = -0.899\ln(x) + 4.996$	logarithmic	0.926	6	-
	1999–2008	$y = 10.46e^{-0.024x}$	exponential	0.935	6	-
	2009–2018	$y = 63.443x^{-0.716}$	power-law	0.812	5	1.716
Kurtosis	1929–1938	$y = 2419.496x^{-1.897}$	power-law	0.993	5	-
	1979–1988	$y = 40.072e^{-0.056x}$	exponential	0.830	4	-
	1989–1998	$y = 43.368x^{-0.654}$	power-law	0.875	6	1.654

Note: The symbol ‘-’ indicates that there is no fractal dimension (d).

Table 6: Fitted equation for the area of hotspots of the krill density distribution.

Index	Period	Fitted equation	Scaling relation	Coefficient of determination (R^2)	Degrees of freedom
Area	1929–1938	$y = 10549.703e^{0.012x}$	exponential	0.924	7
	1979–1988	$y = -3.934x^2 + 1075.542x - 7696.114$	parabolic	0.931	5
	1989–1998	$y = -1.237x^2 + 799.838x - 10691.501$	parabolic	0.940	5
	1999–2008	$y = 16154.41e^{0.008x}$	exponential	0.772	6
	2009–2018	$y = 8800.152e^{0.013x}$	exponential	0.920	7

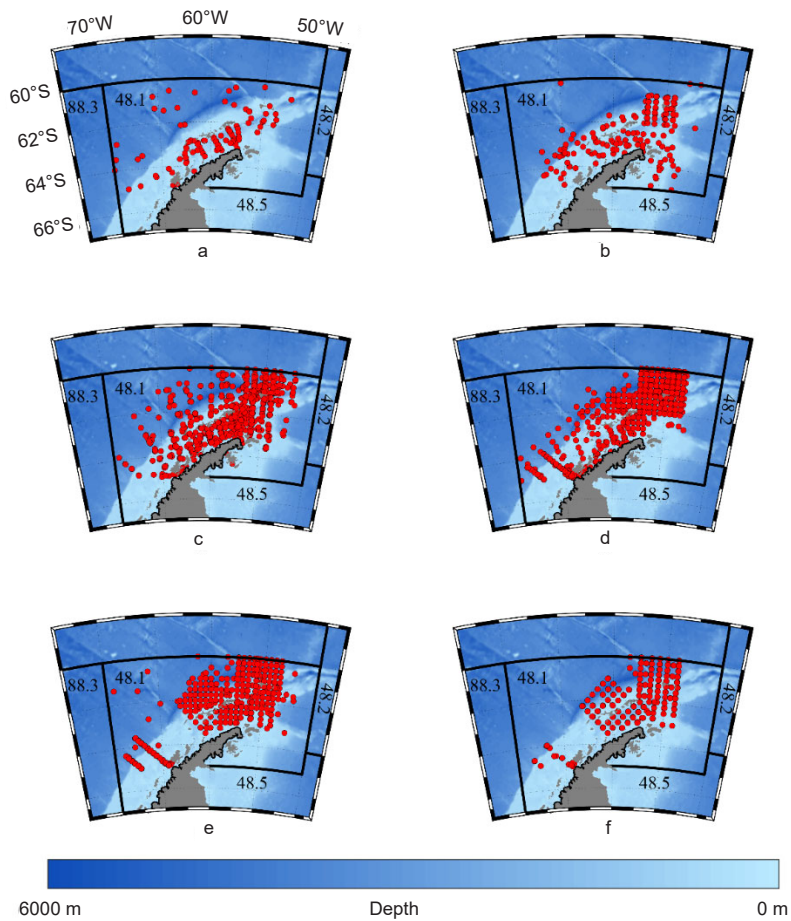


Figure 1: Survey stations for collecting krill density data in the waters around the Antarctic Peninsula. The red circles represent the survey stations. 48.1, 48.2, 48.5 and 88.3 are CCAMLR subareas: (a) 1929–1938; (b) 1969–1978; (c) 1979–1988; (d) 1989–1998; (e) 1999–2008; (f) 2009–2018.

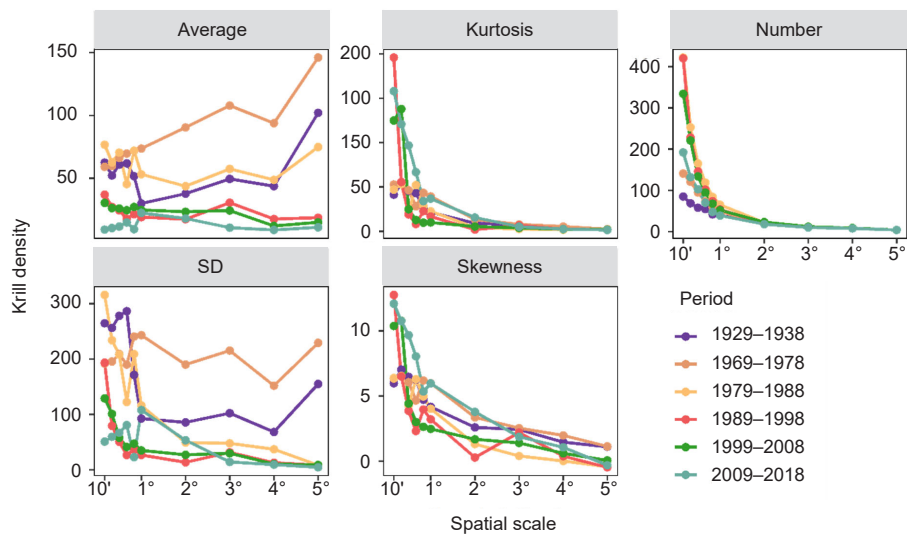


Figure 2: Variation in the indices of krill density for all stations with spatial scale. Average, kurtosis, SD and skewness were used to assess krill density for all patches in each period. SD: standard deviation; number: number of krill patches. Different periods are represented in different colours. 10' represents a spatial scale of $10' \times 10'$.

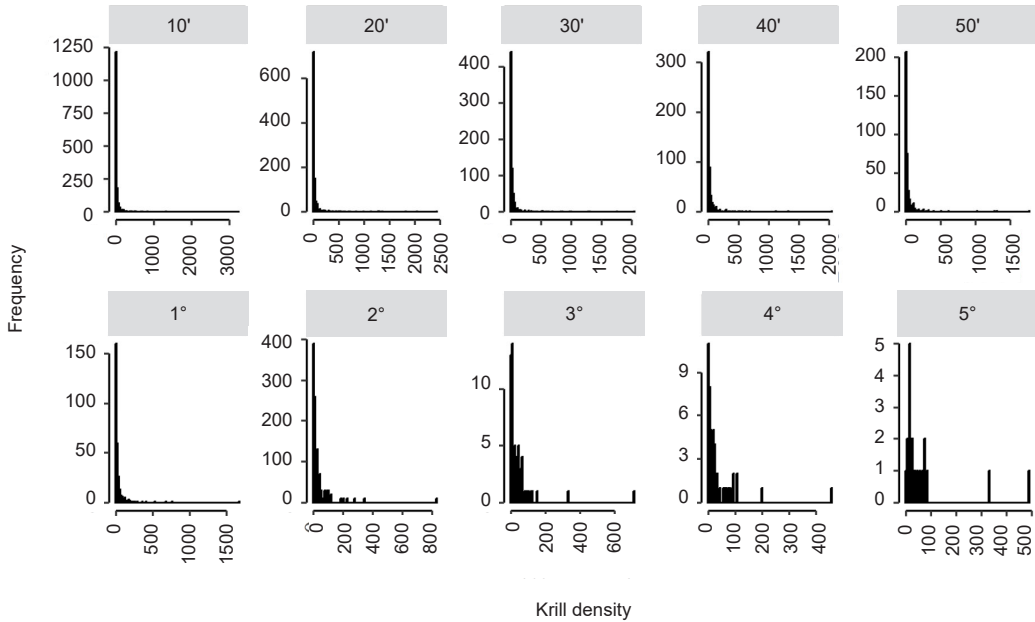


Figure 3: Histograms of the krill density observations for all stations across spatial scales pooled for all years. 10' represents a spatial scale of $10' \times 10'$.

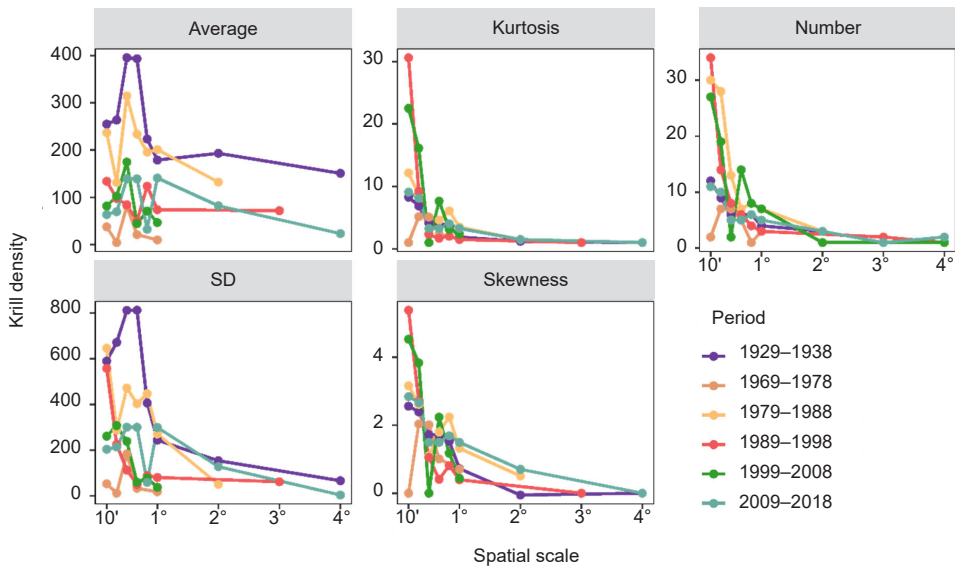


Figure 4: Variation in the nonspatial indices of krill density for hotspots using a spatial scale. Average, kurtosis, SD and skewness were used to assess krill density for all hotspot patches in each period. SD: standard deviation; number: number of krill hotspot patches. Different periods are represented in different colours. 10' represents a spatial scale of $10' \times 10'$.

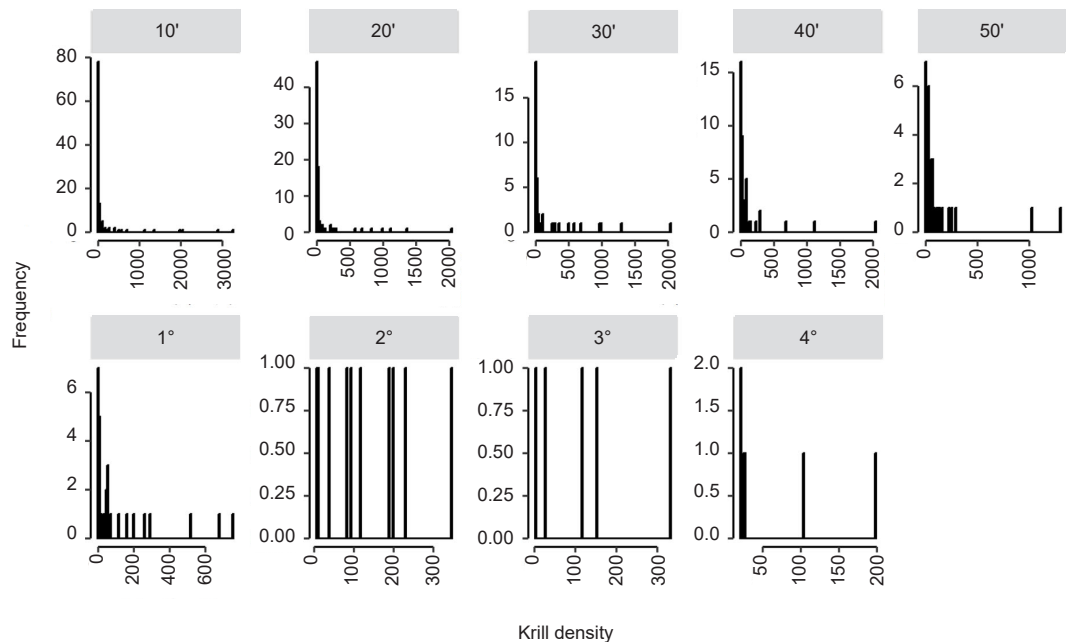


Figure 5: Histograms of the krill density observations for hotspots across spatial scales pooled for all years. 10' represents a spatial scale of $10' \times 10'$.

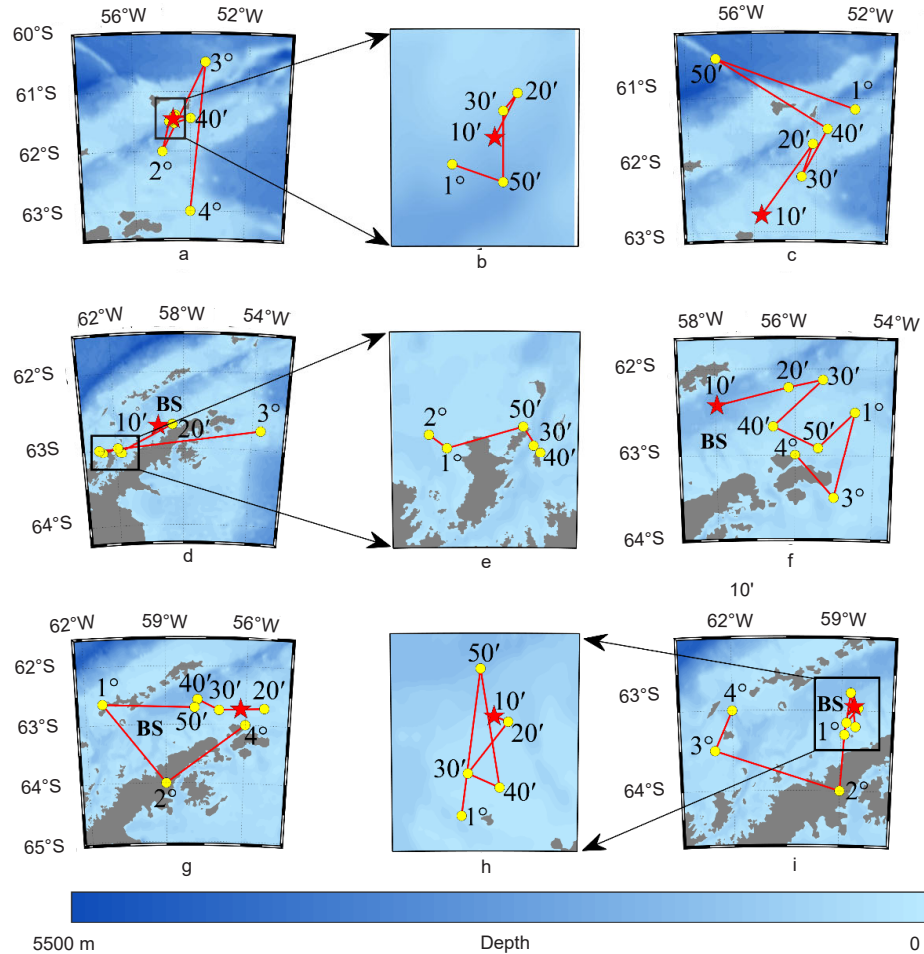


Figure 6: Variation in the centroid of krill density hotspots distribution at different spatial scales. The red asterisks represent the hotspot centroids in a $10' \times 10'$ spatial scale. The yellow circles represent the hotspot centroids at spatial scales other than $10' \times 10'$. $10'$ represents a spatial scale of $10' \times 10'$. 1° represents a spatial scale of $1^\circ \times 1^\circ$. Other numbers have similar meanings. The red lines represent the trajectories of hotspot centroids under different spatial scales: (a) hotspot centroid at all spatial scales from 1929 to 1938; (b) hotspot centroid at spatial scales of $10' \times 10'$, $20' \times 20'$, $30' \times 30'$, $50' \times 50'$ and $1^\circ \times 1^\circ$ between 1929 to 1938; (c) hotspot centroid at all spatial scales from 1969 to 1978; (d) hotspot centroid at all spatial scales from 1979 to 1988; (e) hotspot centroid at spatial scales of $30' \times 30'$, $40' \times 40'$, $50' \times 50'$, $1^\circ \times 1^\circ$ and $2^\circ \times 2^\circ$ from 1979 to 1988; (f) hotspot centroid at all spatial scales from 1989 to 1998; (g) hotspot centroid at all spatial scales from 1999 to 2008; (h) hotspot centroid at spatial scales of $10' \times 10'$, $20' \times 20'$, $30' \times 30'$, $40' \times 40'$, $50' \times 50'$ and $1^\circ \times 1^\circ$ from 2009 to 2018; (i) hotspot centroid at all spatial scales from 2009 to 2018. BS: Bransfield Strait.

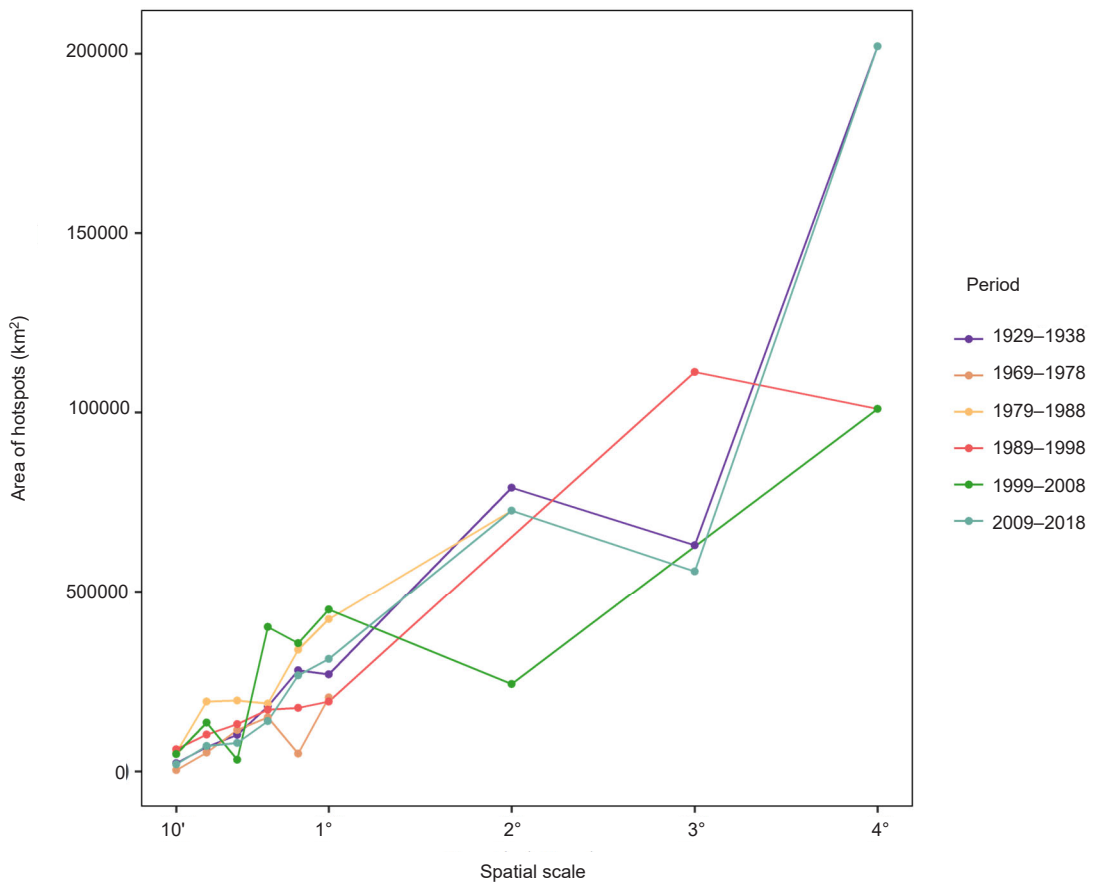


Figure 7: Variation in hotspot areas against the spatial scale. 10' represents a spatial scale of $10' \times 10'$.

Liste des tableaux

- Tableau 1 : Périodes des campagnes d'évaluation et taille des échantillons issus de la collecte des données de densité du krill dans les eaux entourant la péninsule antarctique (source des données : KRILLBASE-ABUNDANCE).
- Tableau 2 : Modèles de régression utilisés pour évaluer l'effet d'échelle des indices. Y représente l'indice ; x représente l'échelle spatiale (l'unité de x est ').
- Tableau 3 : Équations ajustées des indices et des échelles spatiales (l'unité de x est ').
- Tableau 4 : Nombre de regroupements à diverses échelles spatiales au cours de différentes périodes.
- Tableau 5 : Équations ajustées des indices des zones de concentration et des échelles spatiales (l'unité de x est ').
- Tableau 6 : Équations ajustées pour les zones de concentration de la distribution de la densité du krill.

Liste des figures

- Figure 1 : Stations de collecte de données de densité du krill dans les eaux entourant la péninsule antarctique. Les cercles rouges représentent les stations. 48.1, 48.2, 48.5 et 88.3 sont les sous-zones de la CCAMLR : (a) 1929–1938 ; (b) 1969–1978 ; (c) 1979–1988 ; (d) 1989–1998 ; (e) 1999–2008 ; (f) 2009–2018.
- Figure 2 : Variation des indices de densité du krill pour toutes les stations en fonction de l'échelle spatiale. La moyenne (*average*), l'aplatissement (*kurtosis*), l'écart-type (*SD*) et l'asymétrie (*skewness*) ont été utilisés pour évaluer la densité du krill dans tous les regroupements pour chaque période. SD : écart-type ; nombre (*number*) : nombre de regroupements de krill. Les différentes périodes sont représentées par différentes couleurs. 10' représente une échelle spatiale de $10' \times 10'$.
- Figure 3 : Histogrammes des observations de densité du krill pour toutes les stations à toutes les échelles spatiales regroupées.
- Figure 4 : Variation des indices non spatiaux de la densité du krill dans les zones de concentration en utilisant une échelle spatiale. La moyenne (*average*), l'aplatissement (*kurtosis*), l'écart-type (*SD*) et l'asymétrie (*skewness*) ont été utilisés pour évaluer la densité du krill dans tous les regroupements dans les zones de concentration pour chaque période. SD : écart-type ; nombre (*number*) : nombre de zones de concentration de krill. Les différentes périodes sont représentées par différentes couleurs. 10' représente une échelle spatiale de $10' \times 10'$.
- Figure 5 : Histogrammes des observations de densité du krill pour toutes les zones de concentration à toutes les échelles spatiales regroupées pour toutes les années. 10' représente une échelle spatiale de $10' \times 10'$.
- Figure 6 : Variation du centroïde de la distribution de la densité de krill dans les zones de concentration à différentes échelles spatiales. Les astérisques rouges représentent les centroïdes des zones de concentration à une échelle spatiale de $10' \times 10'$. Les cercles jaunes représentent les centroïdes des zones de concentration à des échelles spatiales autres que $10' \times 10'$. 10' représente une échelle spatiale de $10' \times 10'$. 1° représente une échelle spatiale de $1^\circ \times 1^\circ$. D'autres nombres ont des significations similaires. Les lignes rouges représentent les trajectoires des centroïdes des zones de concentration à différentes échelles spatiales : (a) centroïde de la zone de concentration à toutes les échelles spatiales entre 1929 et 1938 ; (b) centroïde de la zone de concentration aux échelles spatiales de $10' \times 10'$, $20' \times 20'$, $30' \times 30'$, $50' \times 50'$ et $1^\circ \times 1^\circ$ entre 1929 et 1938 ; (c) centroïde de la zone de concentration à toutes les échelles spatiales de 1969 à 1978 ; (d) centroïde de la zone de concentration à toutes les échelles spatiales de 1979 à 1988 ; (e) centroïde de la zone de concentration aux échelles spatiales de $30' \times 30'$, $40' \times 40'$, $50' \times 50'$, $1^\circ \times 1^\circ$ et $2^\circ \times 2^\circ$ de 1979 à 1988 ; (f) centroïde de la zone de concentration à toutes les échelles spatiales de 1989 à 1998 ; (g) centroïde

de la zone de concentration à toutes les échelles spatiales de 1999 à 2008 ; (h) centroïde de la zone de concentration aux échelles spatiales de $10' \times 10'$, $20' \times 20'$, $30' \times 30'$, $40 \times 40'$, $50 \times 50'$ et $1^\circ \times 1^\circ$ de 2009 à 2018 ; (g) centroïde de la zone de concentration à toutes les échelles spatiales de 2009 à 2018 ; BS : détroit de Bransfield.

Figure 7 : Variation de l'aire des zones de concentration en fonction de l'échelle spatiale. $10'$ représente une échelle spatiale de $10' \times 10'$.

Таблицы

Табл. 1: Периоды съемок и размеры проб при сборе данных о плотности криля в водах вокруг Антарктического полуострова (источник данных: KRILLBASE-ABUNDANCE).

Табл. 2: Регрессионные модели, использованные для оценки влияния масштабирования на индексы. Y обозначает индекс; x обозначает пространственный масштаб (единица измерения x – это $'$).

Табл. 3: Подогнанные уравнения индексов и пространственных масштабов (единица измерения x – это $'$).

Табл. 4: Количество плотных скоплений в очагах в разных пространственных масштабах в различные периоды.

Табл. 5: Подогнанные уравнения индексов очагов и пространственных масштабов (единица измерения x – это $'$).

Табл. 6: Подогнанное уравнение распределения плотности криля с учетом площади очагов.

Рисунки

Рис. 1: Станции съемок сбора данных о плотности криля в водах вокруг Антарктического полуострова. Станции съемок обозначены красными кружками. Подрайоны 48.1, 48.2, 48.5 и 88.3: (a) 1929–1938 гг.; (b) 1969–1978 гг.; (c) 1979–1988 гг.; (d) 1989–1998 гг.; (e) 1999–2008 гг.; (f) 2009–2018 гг.

Рис. 2: Разброс индексов плотности криля для всех станций в зависимости от пространственного масштаба. Усреднение, эксцесс, стандартное отклонение и асимметрия применялись для оценки распределения плотности криля по всем скоплениям за каждый период. SD: стандартное отклонение; number: количество скоплений криля. Различные периоды выделены разными цветами. $10'$ – это пространственный масштаб $10' \times 10'$.

Рис. 3: Гистограммы наблюдений за плотностью криля со всех станций, сгруппированных по пространственным масштабам.

Рис. 4: Изменение не связанных с пространством показателей плотности криля в очагах по шкале изменения масштаба. Усреднение, эксцесс, стандартное отклонение и асимметрия применялись для оценки распределения плотности криля по всем скоплениям в очагах за каждый период. SD: стандартное отклонение; number: количество скоплений криля в очагах. Различные периоды выделены разными цветами. $10'$ – это пространственный масштаб $10' \times 10'$.

Рис. 5: Гистограммы наблюдений за плотностью криля во всех очагах скоплений, сгруппированных по пространственным масштабам за все годы. $10'$ – это пространственный масштаб $10' \times 10'$.

Рис. 6: Изменение положения центроида очагов скоплений криля в зависимости от пространственного масштаба. Красные звездочки обозначают местонахождение центроида очагов в пространственном масштабе $10' \times 10'$.

Желтые кружки обозначают точки центроида очагов в других пространственных масштабах, отличных от $10' \times 10'$. $10'$ – это пространственный масштаб $10' \times 10'$. 1° – это пространственный масштаб $1^\circ \times 1^\circ$. Другие числовые значения имеют аналогичный смысл. Красные линии представляют собой траектории смещения центроидов очагов скоплений в различных пространственных масштабах: (а) центроиды очагов скоплений во всех пространственных масштабах с 1929 по 1938 гг.; (б) центроиды очагов скоплений в пространственных масштабах $10' \times 10'$, $20' \times 20'$, $30' \times 30'$, $50' \times 50'$ и $1^\circ \times 1^\circ$ между 1929 и 1938 гг.; (с) центроиды очагов скоплений во всех пространственных масштабах с 1969 по 1978 гг.; (д) центроиды очагов скоплений во всех пространственных масштабах с 1979 по 1988 гг.; (е) центроиды очагов скоплений в пространственных масштабах $30' \times 30'$, $40' \times 40'$, $50' \times 50'$, $1^\circ \times 1^\circ$ и $2^\circ \times 2^\circ$ между 1979 и 1988 гг.; (ф) центроиды очагов скоплений во всех пространственных масштабах с 1989 по 1998 гг.; (г) центроиды очагов скоплений во всех пространственных масштабах с 1999 по 2008 гг.; (х) центроиды очагов скоплений в пространственных масштабах $10' \times 10'$, $20' \times 20'$, $30' \times 30'$, $40' \times 40'$, $50' \times 50'$ и $1^\circ \times 1^\circ$ между 2009 и 2018 гг.; (и) центроиды очагов скоплений во всех пространственных масштабах с 2009 по 2018 гг. BS: пролив Брансфилда

Рис. 7: Изменение размеров очагов скоплений в зависимости от пространственного масштаба. $10'$ – это пространственный масштаб $10' \times 10'$.

Lista de tablas

Tabla 1: Períodos de prospección y tamaños de muestra del recabado de datos de la densidad del kril en las aguas alrededor de la península Antártica (base de datos: KRILLBASE-ABUNDANCE).

Tabla 2: Los modelos de regresión utilizados para evaluar el efecto escalar de los índices. Y se refiere al índice; mientras que x se refiere a la escala espacial (la unidad de x es ').

Tabla 3: Ecuaciones ajustadas de índices y escalas espaciales (la unidad de x es ').

Tabla 4: Número de puntos de alta densidad a diferentes escalas espaciales, en diferentes períodos.

Tabla 5: Ecuaciones ajustadas de índices de focos de abundancia y escalas espaciales (la unidad de x es ').

Tabla 6: Ecuación ajustada para el área de los focos de abundancia de la distribución de la densidad del kril.

Lista de figuras

Figura 1: Estaciones de prospección para recabar datos de la densidad del kril en las aguas alrededor de la península Antártica. Los círculos rojos representan las estaciones de prospección. 48.1, 48.2, 48.5 y 88.3 son subáreas de la CCRVMA: (а) 1929–1938; (б) 1969–1978; (с) 1979–1988; (д) 1989–1998; (е) 1999–2008; (ж) 2009–2018.

Figura 2: Variación en los índices de la densidad del kril para todas las estaciones, con escala espacial. Se utilizó la media, la curtosis, la desviación estándar y la asimetría estadística para estudiar la densidad del kril en todos los puntos de alta densidad en cada periodo. SD: desviación estándar; número: número de puntos de alta densidad de kril. Los diferentes períodos están representados en diferentes colores. $10'$ representa una escala espacial de $10' \times 10'$.

Figura 3: Histogramas de las observaciones de la densidad del kril para todas las estaciones en las diferentes escalas espaciales agrupadas.

Figura 4: Variación de los índices de la densidad del kril en los focos de abundancia, con escala espacial. Se utilizó la media, la curtosis, la desviación estándar y la asimetría estadística para estudiar la densidad del kril en todos los focos de puntos de alta densidad en cada periodo. SD: desviación estándar; número: número de focos de puntos de

alta densidad de kril. Los diferentes períodos están representados en diferentes colores. $10'$ representa una escala espacial de $10' \times 10'$.

Figura 5: Histogramas de las observaciones de la densidad del kril en todos los focos de abundancia a todas las escalas espaciales agrupadas, todos los años combinados. $10'$ representa una escala espacial de $10' \times 10'$.

Figura 6: Variación en el centroide de la distribución de los focos de la densidad del kril a diferentes escalas espaciales. Los asteriscos rojos representan los centroides de los focos de abundancia a una escala espacial de $10' \times 10'$. Los círculos amarillos representan los centroides de los focos de abundancia a escalas espaciales distintas a $10' \times 10'$. $10'$ representa una escala espacial de $10' \times 10'$. 1° representa una escala espacial de $1^\circ \times 1^\circ$. Otros números tienen significados similares. Las líneas rojas representan los recorridos de los centroides de los focos de abundancia a diferentes escalas espaciales: (a) centroide del foco de abundancia a todas las escalas espaciales entre 1929 y 1938; (b) centroide del foco de abundancia a escalas espaciales de $10' \times 10'$, $20' \times 20'$, $30' \times 30'$, $50' \times 50'$ y $1^\circ \times 1^\circ$ entre 1929 y 1938; (c) centroide del foco de abundancia a todas las escalas espaciales entre 1969 y 1978; (d) centroide del foco de abundancia a todas las escalas espaciales entre 1979 y 1988; (e) centroide del foco de abundancia a escalas espaciales de $30' \times 30'$, $40' \times 40'$, $50' \times 50'$, $1^\circ \times 1^\circ$ y $2^\circ \times 2^\circ$ entre 1979 y 1988; (f) centroide del foco de abundancia a todas las escalas espaciales entre 1989 y 1998; (g) centroide del foco de abundancia a todas las escalas espaciales entre 1999 y 2008; (h) centroide del foco de abundancia a escalas espaciales de $10' \times 10'$, $20' \times 20'$, $30' \times 30'$, $40' \times 40'$, $50' \times 50'$ y $1^\circ \times 1^\circ$ entre 2009 y 2018; (i) centroide del foco de abundancia a todas las escalas espaciales entre 2009 y 2018. BS: estrecho de Bransfield.

Figura 7: Relación entre las áreas de los focos de abundancia y la escala espacial. $10'$ representa una escala espacial de $10' \times 10'$.

